

Locating environmental charge impurities with confluent laser spectroscopy of multiple quantum dots

M. Hauck,¹ F. Seilmeyer,¹ S. E. Beavan,¹ A. Badolato,² P. M. Petroff,³ and A. Högele¹

¹Fakultät für Physik, Munich Quantum Center, and Center for NanoScience (CeNS), Ludwig-Maximilians-Universität München, 80539 München, Germany

²Department of Physics and Astronomy, University of Rochester, Rochester, New York 14627, USA

³Materials Department, University of California, Santa Barbara, California 93106, USA

(Received 6 October 2014; revised manuscript received 25 November 2014; published 8 December 2014)

We used resonant laser spectroscopy of multiple InGaAs quantum dots to spatially locate charge fluctuators in the surrounding semiconductor matrix. By mapping out the resonance condition between a narrow-band laser and the neutral exciton transitions of individual dots in a field effect device, we identified spectral discontinuities as arising from charging and discharging events that take place within the volume adjacent to the quantum dots. Our analysis suggests that residual carbon dopants are a major source of charge-fluctuating traps in quantum dot heterostructures.

DOI: 10.1103/PhysRevB.90.235306

PACS number(s): 78.67.Hc, 78.55.Cr, 73.21.La

I. INTRODUCTION

The exciton transitions in self-assembled InGaAs quantum dots (QDs) are elementary to potential applications in quantum information processing [1] and quantum cryptography [2]. For quantum cryptography protocols, QDs can be used to generate indistinguishable single photons [3,4] with high repetition rates [5], or to produce entangled photon pairs on demand [6]. In addition, efficient all-optical spin manipulation schemes characteristic of QDs [7] can be exploited for spintronics applications [8]. Recent developments in spin-photon interfacing can also be used to reversibly transfer qubits between light and QD states [9,10] and place QDs alongside the nitrogen-vacancy center in diamond [11] as a potential solid-state building block for practical quantum devices. All these experiments ubiquitously rely on a well defined and stable resonance condition between the exciton transition and the laser fields.

In current QD devices, however, the fidelity of such protocols is limited by spectral fluctuations. Early resonant experiments identified spectral diffusion as a primary limitation to the temporal stability of the resonance condition [12]. More recent studies of resonance fluorescence [13,14] and its dynamics [15] found that the main source of resonance instability is the charge noise due to fluctuations in the electrostatic environment, which is detrimental to the quality of single photons that can be generated in QD devices [16–18]. Recent work on related device heterostructures has identified charge traps at the GaAs/AlGaAs superlattice (SL) interface as a major source of spectral diffusion [19], and similar effects have also been observed in devices without a SL [20]. In this work, we investigate the resonance condition for a number of QDs in a field-effect device, and find that spectral jumps are caused by charge fluctuations occurring in the semiconductor volume surrounding the QDs, and are not purely an interface effect. Using the gate-voltage dependence combined with the magnitude of the spectral fluctuations, we identify the likely source of these charge traps as residual carbon impurities, and the individual impurity sites can be located more precisely when their influence can be observed in more than one QD spectrum. Such spectroscopic studies could be used in the first

instance as a highly sensitive measure of semiconductor purity, and second to adjust the growth methods and heterostructure design so as to reduce the detrimental charge noise in QD devices.

II. EXPERIMENTAL DETAILS

The self-assembled InGaAs QDs studied here were grown by molecular beam epitaxy (MBE) [21] with subsequent annealing, and have emission energies around 1.3 eV. The QDs are embedded in a field-effect structure to allow deterministic control of the charge occupation of the dot [22]. On the “back” side, a 25 nm thick GaAs tunneling barrier separates the QDs from a heavily n^+ doped GaAs layer (thickness 20 nm, doping concentration $4 \times 10^{18} \text{ cm}^{-3}$) which forms the back electrode. The “top” side of the QD layer is covered first by a 30 nm thick GaAs capping layer, and then with an additional AlGaAs/GaAs SL of 116 nm thickness. A 5 nm NiCr layer was evaporated on top of the SL to form the second electrode.

The energy levels of individual QDs were investigated with photoluminescence (PL) [23] and differential transmission (DT) [24] spectroscopy in a confocal microscope setup shown schematically in Fig. 1(a). The sample had a QD density such that there were typically 10–50 QDs in an area corresponding to a diffraction-limited focal spot of $\sim 1 \mu\text{m}$ diameter. Out of this small ensemble, individual QDs were spectrally selected for PL and DT measurements. By applying a gate voltage V_G between the top gate and the back contact, the energy levels of a QD shift relative to the Fermi energy E_F , allowing control over the number of electrons that occupy the dot [22]. Figure 1(b) represents a typical QD PL charging diagram as a function of V_G , showing the neutral exciton (X^0) and the negatively charged exciton (X^{1-}) emission resonances, respectively [23].

The neutral exciton transition was investigated in finer detail for a number of QDs using DT spectroscopy, with the polarization of the excitation laser chosen so as to excite just one of the two exchange-interaction split resonances [12]. Examples of DT spectra are shown in Fig. 1(d). The calculated lifetime-limited linewidth of the X^0 transition is $\sim 0.7 \mu\text{eV}$; however the transition is further broadened due to charge

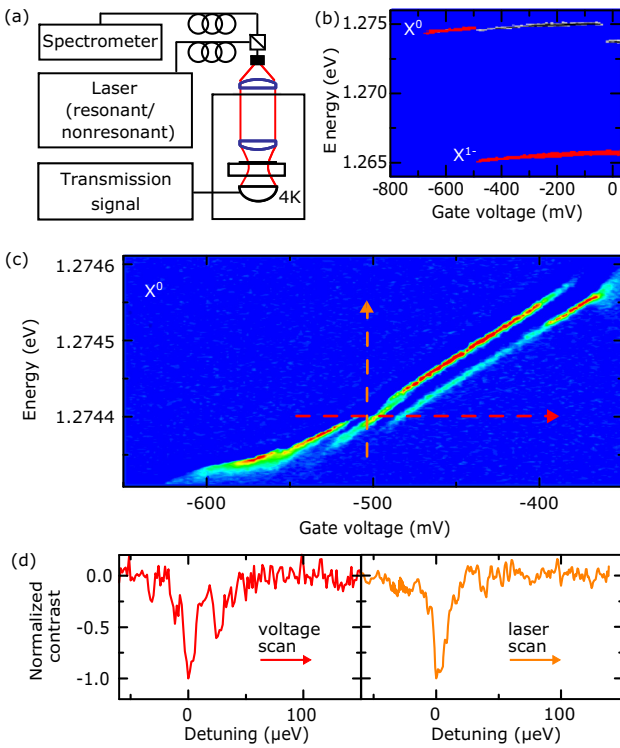


FIG. 1. (Color online) (a) Setup for spectroscopy of a single quantum dot at 4.2 K. For resonant excitation, the transmission is measured by a photodiode underneath the sample. Photoluminescence is measured using a spectrometer. (b) Photoluminescence charging diagram of a quantum dot (QD1) with characteristic X^0 and X^{1-} stability plateaus. (c) High-resolution DT spectroscopy of the X^0 stability plateau for the same dot as in (b). In addition to the linear Stark shift, there are several abrupt changes in the exciton resonance energies as the gate voltage is varied. (d) Normalized DT spectra along the dashed lines shown in (c).

fluctuations in the solid-state matrix surrounding the QD [12,15]. For charge fluctuations that occur on a time scale much faster than the measurement integration times (typically ~ 1 s), the resulting jitter in the QD resonance energy is observed as broadened linewidths in the range 4 ± 2 μeV [12,15].

For a significant fraction of QDs, the linear relationship between the exciton resonance energy and the applied gate voltage is interrupted by several distinct jumps. An example of this effect is apparent in Fig. 1(c). The energy dispersion gradient is consistent across the X^0 transition plateau; however there are discontinuities in energy observed at specific values of V_G . With increasing V_G , the transition energy jumps to lower values by an amount in the range of 7 to 38 μeV . Such spectral discontinuities could be caused by similar environmental charge fluctuations which give rise to exciton line broadening. However, the spectral jumps studied here in more detail occur at specific gate voltages, and correspond to larger resonance-energy shifts in the QD transition. Recently, the work of Houel *et al.* [19] attributed these spectral jumps to discrete charging of potential traps located at the interface to the SL. Our analysis detailed below suggests the presence of additional potential traps in the surrounding GaAs matrix.

III. MODELING AND DISCUSSION

The exciton resonance energy E of a QD is shifted by an electric field \mathbf{F} through the quantum-confined Stark effect:

$$E = E_0 - \mathbf{p} \cdot \mathbf{F} + \beta \cdot \mathbf{F}^2, \quad (1)$$

where E_0 is the unperturbed exciton resonance energy, $\mathbf{p} = p\hat{\mathbf{z}}$ is the static dipole moment of the exciton transition, and β is the polarizability [25]. This relation quantifies how an applied electric field can be used to shift the exciton resonance deterministically, and also encompasses the mechanism through which charge fluctuations in the solid-state matrix surrounding the QD can perturb the resonance [19].

An applied gate voltage V_G generates an electric field $\mathbf{F} = \frac{-(V_G - V_S)}{l}\hat{\mathbf{z}}$, where l is the distance between the n^+ layer and the top surface electrode, and $V_S = 0.62$ V is the Schottky barrier potential [25]. The axial polarizability β_z along the growth direction has been measured for similar dots as ≈ -0.3 $\mu\text{eV}/(\text{kV/cm})^2$ [25]. For the X^0 transition, which occurs with $|V_G + V_S|$ in the range 0.9–1.1 V, the effect of the axial polarizability is negligible compared to the much larger dipole contribution. Therefore, the magnitude of the dipole moment p can be determined from the gradient of the X^0 transition energy versus gate voltage V_G as $p = (\partial E / \partial V_G)l$. Values of p are typically $e \times 0.2$ nm (where e is the elementary charge) for the strongly confining QDs surveyed in this work [25]. In the QD plane, there is no permanent dipole moment; however the larger geometric extent of the dot in this direction implies a much larger lateral polarizability of the order of $\beta_{xy} \approx -4 \mu\text{eV}/(\text{kV/cm})^2$ [26]. Therefore, charge fluctuations in the vicinity of a QD can perturb the exciton resonance by coupling to the permanent dipole moment in the $\hat{\mathbf{z}}$ direction, or through the polarizability in the lateral plane.

The magnitude of the exciton resonance-energy shift caused by a single unit charge q placed near the dot can be determined with a simple electrostatic model of the heterostructure depicted in Fig. 2(c). A QD exciton is represented as a dipole oriented along the $\hat{\mathbf{z}}$ axis, positioned between two electrodes. A charge-trapping site is located at an arbitrary distance from the dot, described by position vector \mathbf{r} . Upon occupation of such a trapping potential, the change in the static electric field, $\Delta\mathbf{F}$, at the QD position is approximated as

$$\Delta\mathbf{F} = \frac{1}{4\pi\epsilon_0\epsilon_r} \left(\frac{q}{|\mathbf{r}|^2} \hat{\mathbf{r}} + \frac{-q}{|\mathbf{r}_{m_1}|^2} \hat{\mathbf{r}}_{m_1} + \frac{-q}{|\mathbf{r}_{m_2}|^2} \hat{\mathbf{r}}_{m_2} \right), \quad (2)$$

where q is a unit charge equal to either $\pm e$, ϵ_0 is the permittivity, ϵ_r is the dielectric constant of the surrounding GaAs matrix, and $\hat{\mathbf{r}} = \mathbf{r}/|\mathbf{r}|$. The first term in the parentheses arises from the impurity charge q . The response of the freely moving charges in the electrodes to the altered charge environment is included (to first order) as second and third terms in the form of image charges m_1 and m_2 , located behind the back gate and top electrode at \mathbf{r}_{m_1} and \mathbf{r}_{m_2} , respectively [see Fig. 2(c)].

Combining Eqs. (1) and (2), the energy shift is obtained as a function of the position and parity of the added charge. As an example, Fig. 2(e) shows the possible positions for added charges of either $\pm e$ that would induce a step change in exciton energy in the range of -10 to -60 μeV , calculated for the QD1

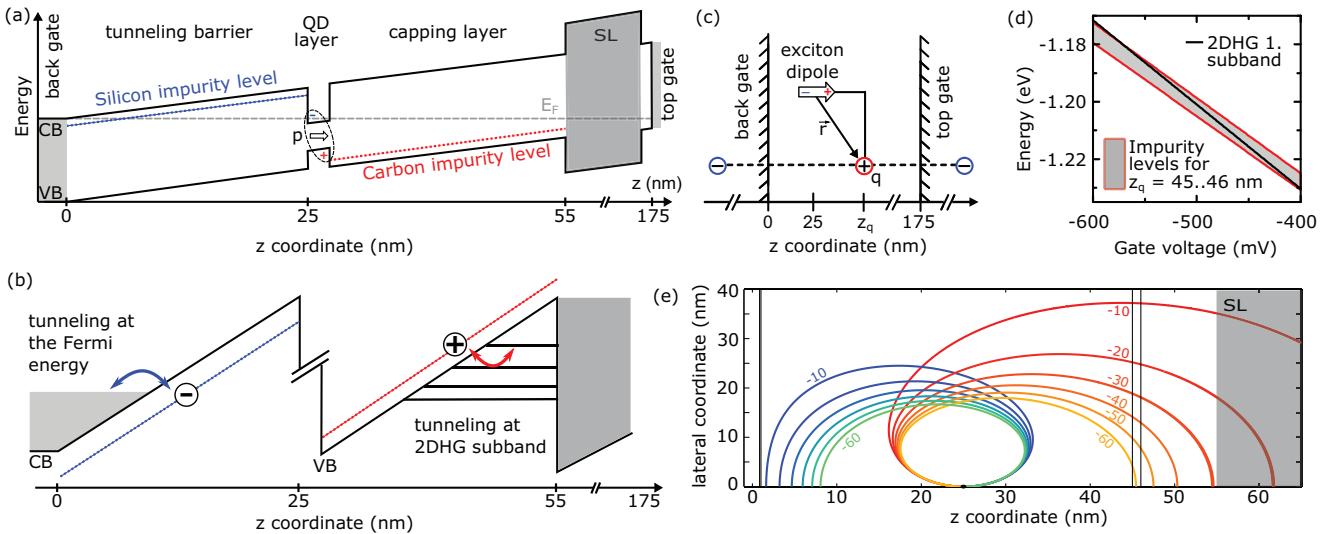


FIG. 2. (Color online) (a) Conduction and valence band edges in the heterostructure device. E_F is the Fermi level, and SL labels the superlattice region, which is scaled down for better visibility of the regions of interest. The QDs are located at $z = 25$ nm. (b) Impurity charging processes that could give rise to the observed energy jumps in the X^0 resonances; an electron-tunneling resonance between a silicon impurity and the back gate (left), or a hole-tunneling resonance between a carbon dopant and a subband in the 2DHG that forms at the interface to the SL (right). (c) The electrostatic model of the heterostructure. The exciton energy is perturbed by an added charge q (here shown to be positive). The effect of the conducting back- and top-gate layers are included to first order in the form of image charges of opposite parity to q (here negative). (d) The resonance condition at the valence band edge between the carbon impurity level and the $n = 1$ subband of the 2DHG. The range of V_G over which the resonance jumps are observed implies that the carbon sites must be located within the $z_q = 45\text{--}46$ nm region. (e) Positions of added charge q that result in specific values of energy shift ΔE . The contour lines are labeled with the value of ΔE in μeV , where the orange-red lines are solutions for $q = +e$, and the green-blue lines correspond to $q = -e$. The gray lines of constant z indicate the regions where there are tunnel resonances for either the silicon or carbon impurity sites. It is important to note that only the carbon impurities exhibit an overlap between the tunnel-resonance V_G range and the Stark-shift ΔE range, and that this region of overlap is not at the interface to the SL.

in Fig. 1 with $p = e \times 0.208$ nm. At large axial distances, the energy jumps could be caused by either a negative charge appearing below the dot, or a positive charge appearing above the dot; i.e., the observed charging events produce an electric field which opposes the externally controlled field. In the lateral plane, the addition of either parity charge could induce such an energy shift. Aside from the magnitude of the energy jumps, their gate voltage dependence is also central to identifying the charge impurity location. Since the spectral jumps occur at specific gate voltages, this suggests that the individual trap sites are tuned through tunnel resonances with charge reservoirs as V_G is varied.

On the lower side of the dot, the most likely source of the electron-trapping sites are the silicon (Si) donor dopants. The n^+ back gate consists of heavily Si-doped GaAs, and previous studies have shown that Si atoms diffuse during the growth process up to several tens of nm along the growth direction of the sample [27]. The energy level associated with the Si donor electron lies $E_{\text{Si}} = 5.8$ meV below the GaAs conduction band edge [28], and the possible V_G -controlled tunneling mechanism is a resonance with the Fermi level in the back gate [see Fig. 2(b)]. A Si impurity site with z in the range 0.85 to 1.0 nm would be consistent with the observed energy jumps occurring within the gate-voltage range of -600 to -400 mV. However, a change of $-e$ at this location would induce a QD resonance-energy shift less than 7 μeV [see Fig. 2(c)]. Such an energy shift is barely resolvable within

the X^0 linewidth, and indeed all the observed discontinuities investigated here have a larger change in energy. Therefore, we can exclude Si impurities as the origin for the observed spectral jumps.

In the region above the QD layer, carbon (C) atoms are the likely source of hole-trapping sites. There is inevitably a residual background C doping in any MBE grown device, and the concentration is known to be on the order of 10^{15} cm^{-3} for our sample. The C acceptor atoms have an energy level $E_C = 26$ meV above the valence band [29]. The V_G -controlled tunneling resonance in this case involves a subband in the two-dimensional hole gas (2DHG) that forms at the interface to the AlGaAs/GaAs SL [depicted in Fig. 2(b)]. The energy of the n th subband in the 2DHG is given by [30]

$$E_{\text{hole}}^n = E_{\text{gap}} + E_{\text{2DHG}} - c_n \left[\frac{(e\hbar)^2}{2m} F^2 \right]^{1/3}, \quad (3)$$

where E_{gap} denotes the GaAs band-gap energy, $E_{\text{2DHG}} = e(V_G - V_S)/z_{\text{2DHG}}$ is the valence band energy at the position of the 2DHG, c_n is the n th Airy coefficient approximated by $c_n \approx [\frac{3}{2}\pi(n - \frac{1}{4})]^{\frac{1}{3}}$, and the effective mass $m = 0.57$ [31]. The carbon charge-trap energy as well as E_{hole}^1 as a function of V_G are shown in Fig. 2(d), identifying resonance conditions in the V_G range from -600 to -400 mV for a carbon atom with z in the interval of 45–46 nm. These z boundaries are depicted in Fig. 2(e) to highlight the fact that a charge of $+e$ located within

this z slice can indeed induce energy shifts up to -60 μ eV. This location of the charge traps is well within the GaAs capping layer and does not coincide with the interface to the SL [19]. Remarkably, however, our results are consistent with the observation that an increase of the separation between the QD layer and the SL is sufficient to inhibit spectral jumps in the plateau of X^0 and favor the narrowing of the exciton resonance [19]. The displacement of the SL to larger values of z implies a change in the resonance condition between the C-impurity level and the lowest 2DHG subband through z_{2DHG} in Eq. (3) such that carbon impurity sites would effectively be depopulated at gate voltages characteristic of the X^0 stability regime.

A. Impurity-site charging dynamics

The spectra of the X^0 transition for the dots surveyed in the course of this work exhibited in general a more complex structure than would be expected from the simplistic model described above. The model explains the majority of spectral jumps, where the QD transition energy changes abruptly from one value to a lower one within a V_G span of 5 to 10 mV. This overlap in gate voltage of the QD energies corresponding to charged and uncharged impurity states is indicative of the rate at which hole-tunneling occurs between the impurity site and the 2DHG. A fast tunneling process yields a small overlap in V_G and vice versa, analogous to the overlaps observed in PL charging diagrams of QDs in samples with different thicknesses of the tunneling barrier between the QD and the Fermi reservoir and correspondingly different electron tunneling rates. In addition to the “sharp” transitions in the charge state of the impurity site, we observe in our DT data instances where an impurity site coexists in both charged and uncharged configurations over an extended gate voltage range of 50 to 100 mV. An example of such a coexistence can be seen in Figs. 1(c) and 3(a) for V_G between -480 mV and -400 mV. This behavior is inexplicable within the modeling framework developed above. A refined model should take into account not only resonant tunneling between the impurity site and the 2DHG, but also dynamic charge capture processes that occur in the presence of an optically generated charge reservoir [20].

To qualitatively understand the impurity site charging dynamics, we adopt the rate-equation formalism of Ref. [20] to determine the time-averaged steady-state occupation of the impurity site N_i as

$$N_i = \frac{1}{1 + \gamma_e/\gamma_c}, \quad (4)$$

where γ_c and γ_e denote the rates at which a hole is captured in, or escapes from, the impurity trap, respectively. In the simple case that was modeled above, $\gamma_e \gg \gamma_c$ when the impurity site is energetically higher than the $n = 1$ subband of the 2DHG, and $N_i \rightarrow 0$. Conversely, when the gate voltage is tuned such that the impurity site is below the lowest 2DHG subband, then $\gamma_e \ll \gamma_c$, and $N_i \rightarrow 1$. However, the capture rate γ_c can also be influenced by the excitation of charge carriers in the QD. Previous investigations have shown that the tunneling rate of holes from a QD is significantly enhanced as it is tuned through resonances with energy levels in the 2DHG [32]. It is possible, therefore, for holes to tunnel from the QD to an $n > 1$ level of the 2DHG, and then occupy the impurity site

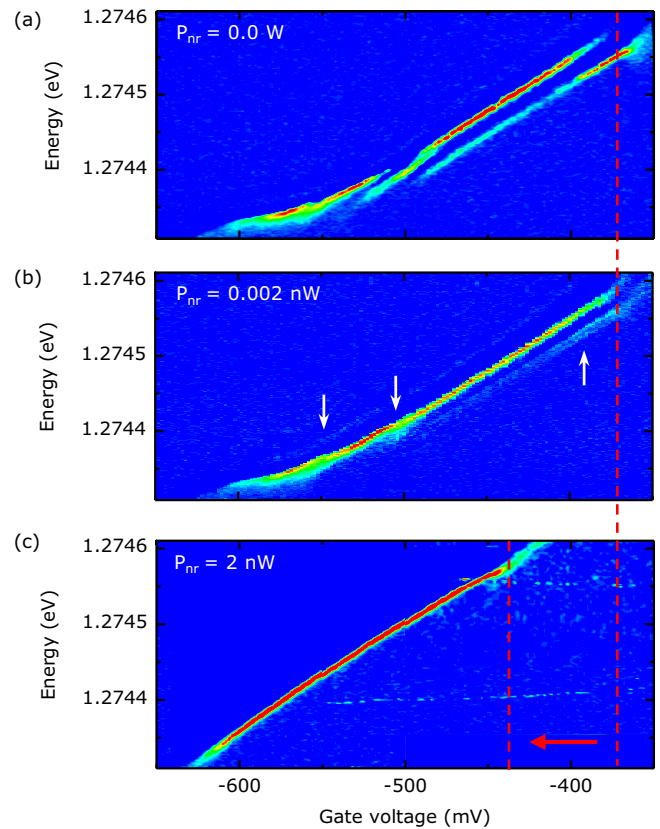


FIG. 3. (Color online) X^0 stability plateaus of the QD1 recorded in DT with an additional nonresonant laser at (a) zero and (b) low ($P_{\text{nr}} = 0.002$ nW) and (c) high ($P_{\text{nr}} = 2$ nW) power. (b) The nonresonant laser at 850 nm photogenerates charge carriers in the wetting layer which yield reduced spectral jumps (indicated by white arrows) due to partial saturation of the charge-trap impurities. (c) At high nonresonant laser powers the charge impurities are fully saturated and the plateau is free of spectral discontinuities. Additionally, the accumulation of photoinduced holes at the superlattice results in a shift of the stability plateau (indicated by the red arrow) due to a partial screening of the gate voltage.

before finally relaxing to the energetically favorable $n = 1$ state of the 2DHG. These QD-DHG resonances effectively enhance γ_c such that it becomes comparable to γ_e (determined only by the valence band properties), and therefore it becomes feasible for the impurity-site to be partially occupied over an extended V_G range, despite not being resonant itself with the 2DHG state. The QD-2DHG resonances observed in similar heterostructures were measured to occur over a range of ≈ 100 mV in V_G [32], in agreement with the V_G span in which we observe intermediate values of N_i .

We can further dynamically perturb the charge environment of the system with the use of nonresonant optical excitation [19,34]. In addition to the resonant laser, the output of an 850 nm laser diode is directed onto the sample, which excites electron-hole pairs in the wetting layer. The effect of this additional charge-carrier generation on the QD charge sensing phenomena is twofold, first altering the electrostatic response of the QD and second directly influencing N_i . The first of these

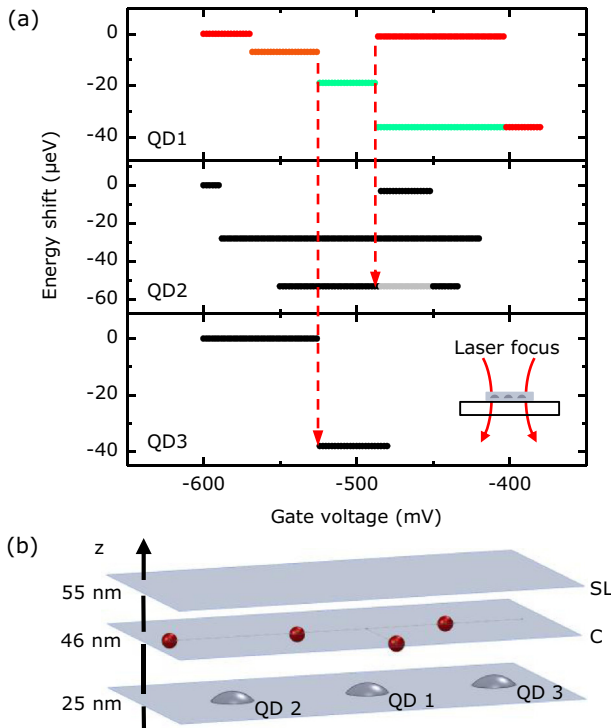


FIG. 4. (Color online) (a) Plateau of the neutral exciton for three different quantum dots. The linear Stark shift is subtracted for clarity. All three quantum dots are situated within one common laser spot (inset lowest panel). QD1 shows three distinct jumps in the exciton dispersion, QD2 has two and QD3 features one discontinuity. QD1 and QD2 have one jump in common which is at a gate voltage of -485 mV and for QD1 and QD3 a joint discontinuity at -526 mV is observed. (b) 3D model of the three quantum dots with corresponding impurities assuming that only carbon states participate. This is only one possible configuration as the angles φ between the quantum dots and impurity cannot be determined. Impurities are red and the quantum dots are gray.

effects is due to a buildup of holes in the 2DEG, which are generated in the wetting layer, but due to the energy-gradient across the heterostructure, tend to relax into the 2DHG. This accumulation of positive charge at the interface to the SL has the effect of partially screening the dot from the externally applied field (causing the well known energy shift of the exciton plateau [33]) as well as screening the QD from the impurity charge. Consequently the spectral jumps decrease monotonically in magnitude with increased nonresonant laser power (see Fig. 3). The effectiveness of the screening depends on the charge density of the 2DHG, and therefore is determined by the laser power. In the limit of high charge density, we can modify the electrostatic model to include the response of the 2DHG in the form of an additional mirror charge. With this modification, an energy jump in the QD spectra of 30 μeV in the absence of nonresonant light is reduced to just 16 μeV . In addition to this electrostatic shielding, the second effect of nonresonant excitation is the direct influence on N_i [20]. The capture rate γ_c is increased with P_{pump} , and beyond a certain saturation power $N_i \rightarrow 1$, despite the impurity trap not

being energetically favorable compared to the $n = 1$ level of the 2DHG. This dynamic saturation effect can be observed in Fig. 3(c).

B. Single impurity sensed with multiple QDs

The transverse location of an impurity site cannot be pinpointed with just one QD sensor; however further constraints can be obtained by using multiple QDs within the impurity vicinity. The absorption spectra of three different QDs (labeled as QD1 to QD3) within a common focal spot (of $\sim 1\text{ μm}$ in diameter) are shown in Fig. 4(a), with the background linear Stark shift subtracted for clarity. It can be seen that there are concurrent spectral jumps occurring for two different QDs at the same gate voltage V_G , which are likely caused by one single impurity. For the spectral jumps which only occur in a single spectrum we assume the charge-trapping sites are too far away from the alternate dots for the spectral effects to be resolved.

As a specific example of the charge-sensing capability, we determine the location of the impurity site that causes jumps in the spectra of QD1 and QD3. The z position of the charge impurity is calculated (using $V_G = 528.5 \pm 3\text{ mV}$) as $z_q = 46.0 \pm 0.5\text{ nm}$. The magnitude of the energy jump in the QD1 spectrum is $\Delta E = 12 \pm 2\text{ μeV}$, while for QD2 the energy change is $\Delta E = 38 \pm 2\text{ μeV}$. The measured dipole moments for each of these dots ($p = e \times 0.180\text{ nm}$ and $e \times 0.208\text{ nm}$ for QD1 and QD3, respectively) determine the transverse location of the impurity site as $29.4 \pm 6.3\text{ nm}$ from QD1, and $12.2 \pm 3.0\text{ nm}$ from QD3. If the relative locations of the QDs were known, there would be a unique solution for the location of the charge impurity. This concurrent sensing concept is depicted in Fig. 4(b), showing the QDs linearly aligned, and a number of carbon impurity sites in the GaAs volume between the QD layer and the SL.

IV. CONCLUSION

In summary, we have identified the cause of spectral jumps in the neutral exciton transitions of QDs as being due to charging of carbon impurity sites. Our results suggest these impurities are located in the semiconductor region surrounding the QD layer. This is further reinforced by measuring the spectral signatures of the charge trapping concurrently for more than one QD. Despite the fact that the charge trapping sites are not themselves at the interface, our analysis suggests that moving the SL interface further from the dot layer would still improve the exciton resonance stability, by shifting the tunnel resonances to different gate voltages.

ACKNOWLEDGMENTS

We acknowledge funding by the Deutsche Forschungsgemeinschaft (SFB 631 and the German Excellence Initiative via the Nanosystems Initiative Munich, NIM) and support from the Center for NanoScience (CeNS).

- [1] A. Imamoğlu, D. D. Awschalom, G. Burkard, D. P. DiVincenzo, D. Loss, M. Sherwin, and A. Small, *Phys. Rev. Lett.* **83**, 4204 (1999).
- [2] A. J. Shields, *Nat. Photonics* **1**, 215 (2007).
- [3] C. Santori, D. Fattal, J. Vucković, G. S. Solomon, and Y. Yamamoto, *Nature (London)* **419**, 594 (2002).
- [4] O. Gazzano, S. Michaelis de Vasconcellos, C. Arnold, A. Nowak, E. Galopin, I. Sagnes, L. Lanco, A. Lemaître, and P. Senellart, *Nat. Commun.* **4**, 1425 (2013).
- [5] P. Michler, A. Kiraz, C. Becher, W. V. Schoenfeld, P. M. Petroff, L. Zhang, E. Hu, and A. Imamoğlu, *Science* **290**, 2282 (2000).
- [6] R. M. Stevenson, R. J. Young, P. Atkinson, K. Cooper, D. A. Ritchie, and A. J. Shields, *Nature (London)* **439**, 179 (2006).
- [7] M. Atatüre, J. Dreiser, A. Badolato, A. Högele, K. Karrai, and A. Imamoğlu, *Science* **312**, 551 (2006).
- [8] R. J. Warburton, *Nat. Mater.* **12**, 483 (2013).
- [9] W. B. Gao, P. Fallahi, E. Togan, A. Delteil, Y. S. Chin, J. Miguel-Sánchez, and A. Imamoğlu, *Nat. Commun.* **4**, 2744 (2013).
- [10] K. De Greve, L. Yu, P. L. McMahon, J. S. Pelc, C. M. Natarajan, N. Y. Kim, E. Abe, S. Maier, C. Schneider, M. Kamp *et al.*, *Nature (London)* **491**, 421 (2012).
- [11] W. Pfaff, B. J. Hensen, H. Bernien, S. B. van Dam, M. S. Blok, T. H. Taminiau, M. J. Tiggelman, R. N. Schouten, M. Markham, D. J. Twitchen *et al.*, *Science* **345**, 532 (2014).
- [12] A. Högele, S. Seidl, M. Kroner, K. Karrai, R. J. Warburton, B. D. Gerardot, and P. M. Petroff, *Phys. Rev. Lett.* **93**, 217401 (2004).
- [13] A. Muller, E. B. Flagg, P. Bianucci, X. Y. Wang, D. G. Deppe, W. Ma, J. Zhang, G. J. Salamo, M. Xiao, and C. K. Shih, *Phys. Rev. Lett.* **99**, 187402 (2007).
- [14] A. N. Vamivakas, Y. Zhao, C. Lu, and M. Atatüre, *Nat. Phys.* **5**, 198 (2009).
- [15] A. V. Kuhlmann, J. Houel, A. Ludwig, L. Greuter, D. Reuter, A. D. Wieck, M. Poggio, and R. J. Warburton, *Nat. Phys.* **9**, 570 (2013).
- [16] H. S. Nguyen, G. Sallen, C. Voisin, P. Roussignol, C. Diederichs, and G. Cassabois, *Appl. Phys. Lett.* **99**, 261904 (2011).
- [17] C. Matthiesen, A. N. Vamivakas, and M. Atatüre, *Phys. Rev. Lett.* **108**, 093602 (2012).
- [18] J. H. Prechtel, A. V. Kuhlmann, J. Houel, L. Greuter, A. Ludwig, D. Reuter, A. D. Wieck, and R. J. Warburton, *Phys. Rev. X* **3**, 041006 (2013).
- [19] J. Houel, A. V. Kuhlmann, L. Greuter, F. Xue, M. Poggio, B. D. Gerardot, P. A. Dalgarno, A. Badolato, P. M. Petroff, A. Ludwig *et al.*, *Phys. Rev. Lett.* **108**, 107401 (2012).
- [20] H. S. Nguyen, G. Sallen, M. Abbarchi, R. Ferreira, C. Voisin, P. Roussignol, G. Cassabois, and C. Diederichs, *Phys. Rev. B* **87**, 115305 (2013).
- [21] D. Leonard, M. Krishnamurthy, C. M. Reaves, S. P. Denbaars, and P. M. Petroff, *Appl. Phys. Lett.* **63**, 3203 (1993).
- [22] H. Drexler, D. Leonard, W. Hansen, J. P. Kotthaus, and P. M. Petroff, *Phys. Rev. Lett.* **73**, 2252 (1994).
- [23] R. J. Warburton, C. Schaflein, D. Haft, F. Bickel, A. Lorke, K. Karrai, J. M. Garcia, W. Schoenfeld, and P. M. Petroff, *Nature (London)* **405**, 926 (2000).
- [24] B. Alen, F. Bickel, K. Karrai, R. J. Warburton, and P. M. Petroff, *Appl. Phys. Lett.* **83**, 2235 (2003).
- [25] R. J. Warburton, C. Schulhauser, D. Haft, C. Schaflein, K. Karrai, J. M. Garcia, W. Schoenfeld, and P. M. Petroff, *Phys. Rev. B* **65**, 113303 (2002).
- [26] B. D. Gerardot, S. Seidl, P. A. Dalgarno, R. J. Warburton, D. Granados, J. M. Garcia, K. Kowalik, O. Krebs, K. Karrai, A. Badolato *et al.*, *Appl. Phys. Lett.* **90**, 041101 (2007).
- [27] N. A. J. M. Kleemans, J. van Bree, A. O. Govorov, J. G. Keizer, G. J. Hamhuis, R. Nötzel, A. Y. Silov, and P. M. Koenraad, *Nat. Phys.* **6**, 534 (2010).
- [28] V. A. Karasyuk, D. G. S. Beckett, M. K. Nissen, A. Villemaire, T. W. Steiner, and M. L. W. Thewalt, *Phys. Rev. B* **49**, 16381 (1994).
- [29] R. Heilman and G. Oelgart, *Semicond. Sci. Technol.* **5**, 1040 (1990).
- [30] J. H. Davies, *The Physics of Low-Dimensional Semiconductors* (Cambridge University Press, Cambridge, 1998).
- [31] N. Bouarissa and H. Aourag, *Infrared Phys. Technol.* **40**, 343 (1999).
- [32] S. Seidl, M. Kroner, P. Dalgarno, A. Högele, J. Smith, M. Ediger, B. Gerardot, J. García, P. Petroff, K. Karrai *et al.*, *Phys. Rev. B* **72**, 195339 (2005).
- [33] J. M. Smith, P. A. Dalgarno, B. Urbaszek, E. J. McGhee, G. S. Buller, G. J. Nott, R. J. Warburton, J. M. Garcia, W. Schoenfeld, and P. M. Petroff, *Appl. Phys. Lett.* **82**, 3761 (2003).
- [34] H. S. Nguyen, G. Sallen, C. Voisin, P. Roussignol, C. Diederichs, and G. Cassabois, *Phys. Rev. Lett.* **108**, 057401 (2012).